https://doi.org/10.18321/1098

Modeling and Simulation of Janus-like Nanoparticles Formation by Solid-Gas Exothermic Reactions

A.A. Markov[1] and K.S. Martirosyan[2]*

[1]Ishlinsky Institute for Problems in Mechanics of the Russian Academy of Sciences, Moscow, 119526, Russia
[2]Department of Physics and Astronomy, University of Texas at Rio Grande Valley, Brownsville, TX 78520, USA

Article info

Received:
16 February 2021

Received in revised form:
10 April 2021

Accepted:
18 June 2021

Keywords:
Ceramic materials
CCSO
Janus-like particles
Porosity development

Abstract

Theoretical model for the simulation of synthesis of Janus-like particles (JP) consisting two different phases using the Carbon Combustion Synthesis of Oxides (CCSO) is presented. The model includes the variation of sample initial porosity, carbon concentration and oxygen flow rate used to predict the formation of JP features. The two temperature (2T) combustion model of chemically active submicron-dispersed mixture of two phases including ferroelectric and ferromagnetic was implemented and assessed by using the experimentally estimated activation energy of 112±3.3 kJ/mol and combustion temperature. The experimental values allowed to account the thermal and concentration expansion effect along with the dispersion by the slip-jump simulation for high Knudsen numbers. The model predicted that the smaller initial porosity of the combustion media creates higher formation rate of Janus-like particles. The simulation of slippage and jumps of the gas temperature allowed the scale-bridging between macro- and micro- structures.

1. Introduction

Janus particles are special types of asymmetric particles whose surfaces have two or more distinct physical properties and chemical compositions within a single particle [1–3]. Over the past decade, various strategies have been developed for the fabrication of Janus particles, including surface coating and nucleation, self-assembly, phase separation, immobilization, microfluidics and others [4–7]. This asymmetric structure gives unique multifunctional properties and functionalization. Recently, carbon combustion synthesis of oxides (CCSO) was applied for quick and energy efficient production of multiferroic composite of cobalt ferrite and barium titanate to form Janus-like particles (JP) matrix structure [8]. It was shows that the exothermic oxidation of carbon nanoparticles with an average size of 5 nm and a specific surface area of 110 m^2/g generates a self-propagating thermal wave with peak temperature of up to 1000 °C. The thermal front rapidly propagates through the mixture of two phases magnetic – $CoFe_2O_4$ and ferroelectric – $BaTiO_3$ to form a nanocomposite structure with Janus like particles. The $BaTiO_3$–$CoFe_2O_4$ magnetoelectric composites are of great technological interest for their potential applications in microwave devices, antennae, sensors, transducers, data storage and controlled release of anti-HIV drug delivery and Alzheimer's, Parkinson's disease treatment [9–12].

The activation energy of the carbon combustion synthesis of Janus-like particles estimated to be 112±3.3 kJ/mol, indicating that the barium titanate and cobalt ferrite presence decrease the activation energy barrier of carbon oxidation and facilitate the ignition process of the combustion synthesis [8]. Existence of discrete $CoFe_2O_4$ and $BaTiO_3$ phases in the composites nanostructures was confirmed using X-ray powder diffraction along with the SEM and TEM analysis. The CCSO is significantly simpler, faster, and more energy efficient as compared to calcination processes that require prolong annealing (hours) at high temperatures. It is observed that the synthesized samples show magnetoelectric coupling on multiferroic cobalt ferrite and barium titanate ceramic composites [8, 12].

*Corresponding author.
E-mail: karen.martirosyan@utrgv.edu

Experimental studies of convective and diffusion transfer in the carbon nanotubes [13–15] have shown that the transfer is accelerated by 2–3 orders of magnitude and more in comparison with estimates based on the theory of a continuous medium. The slippage of a viscous liquid flow on solid wall means nonzero velocity on the boundary. Liquid slip in micro- and nanofluidic discussed in [13]. Gas-dynamic flows in channels with small geometric dimensions exhibit special properties that differ from those of flows in large-sized channels. The main condition for the "smallness" of the channel size is the Knudsen criterion [13], which is equal to the ratio of the mean free path of gas molecules between collisions λ to the channel diameter or to some other characteristic spatial scale of the flow L or to some other characteristic spatial scale of the flow.

The commensurability of these values or significant excess of λ over L means a small diameter of the channel or rarefaction of the gas. The Knudsen layer on porous surface considered in [16, 17]. The phenomenon of intensification of transfer can be partially explained by direct modeling of the motion of an ensemble of molecules by using molecular dynamics (MD) simulations [18]. It should be noted that the mean free path of gas molecules in the pores of carbon exceeds the pore diameter. Collisions of molecules with a nanotube boundary dominate over collisions of molecules with each other. Knudsen numbers reach up to 10–70.

The temperature and concentration jumps of gas flow on solid boundary in submicron channel reported in [19]. On submicron scales, models with slip conditions in combination with jumps in gas concentrations and temperatures on the surface of an isolated tube or in pores are constructed in [20–25]. The processes of propagation of combustion waves were studied with the application of production of solid phase particles by self-propagating high-temperature synthesis (SHS) and CCSO [24–25]. A self-consistent method for calculating heat and mass transfer processes on macro and micro scales has been developed. Various applications of CCSO models for self-consistent calculation of micro- and macro-processes at sufficiently small Knudsen numbers were described [26]. The features of the influence of slip processes, temperature jumps and concentrations of the gas phase components on the propagation of the combustion wave and the synthesis of nickel-zinc ferrite in a channel with a cooled side wall and pores of submicron diameter have been studied. The effects of gas slippage, gas temperature jump and concentrations jumps due to fluxes of O_2, N_2 and CO_2 components on the pore surface are included in the consideration. The muss fluxes of gas flow from the combustion zone and from the sample as a whole causes heat loss and slows down the combustion process during sliding [21–25].

In this report, we generalized the two-temperature model [20, 21] on investigation the thermal and mass dispersion and expansion effect on synthesis JP via CCSO in porous media. The governing system of equations includes the Navier-Stokes equations for the gas phase and along with the thermo-elasticity equations using the Duhamel-Neumann relations. The equations of conservation of mass, momentum and energy using the tensors of mass and thermal dispersion, conductive and convective transfer are applied. The results of simulating the effect of thermal and concentration expansion on porosity distribution in the process of the synthesis of micron JP powders during CCSO are also presented. A dimensionless form of the constitutive equations with similarity parameters was used for calculations, including the effect of dispersion, pore tortuosity coefficient, particle diameter, and local values of Peclet numbers. The formula of unsteady porosity is generalized for JP synthesis at a given distribution of porosity at the initial time instance for the numerical simulation of porous magneto-electric composite materials. The performance and reliability of these materials is influenced by defects or pores, which can arise during the consolidation process. We analyze the impact of pores on the rate of Janus particles sintering via CCSO in the synthesis of polycrystalline multiferroic JP composite from ferroelectric $BaTiO_3$ and ferromagnetic $CoFe_2O_4$. The model of slip processes and jumps of the gas and solid temperatures were employed for scale-bridging between macrostructures and microstructures. We discuss the influence of pores in two-phase combustion on composites by analyzing numerical examples. The inhomogeneous macrostructure concentration and the rate of multiferroic composite formation are numerically investigated for different porosity of carbon, ferroelectric $BaTiO_3$ and ferromagnetic $CoFe_2O_4$ with carbon mixture.

Modeling the synthesis of complex oxide particles was developed in [20, 21] with the approximation of constant pore sizes, given a priori. It should be noted that the pore sizes, as a rule, are unevenly distributed in the reactor of synthesis and have been changed over the time, affecting the mass and heat fluxes of reactants and products through the porous

medium. Temperature and concentration gradients lead to change across the volume and the appearance of displacements and stresses in the solid phase, leading to pores change in space and time. In the present paper, the model simulation of Janus like particles is developed by implementing porosity variables as well as thermal and mass dispersion in a porous media. We restricted ourselves to the study of densification using the thermal elasticity theory [26]. The sintering simulation using a non-linear viscous material theory [27] is not considered.

2. Micro- and macroscale modeling

The dynamics of the heat and mass transfer at submicron scale strongly depend on so called slippage. A self-consistent method of computation of heat and mass transfer at micro- and macroscales was developed [20]. Modeling the synthesis of materials by CCSO [24, 25] were developed in the approximation of the permanent sizes of the pores. Physically, a porous medium is formed by a solid phase and one or more fluid phases. The solid may have a periodic or random structure, each phase may be continuous or dispersed and the characteristic sizes of the geometric heterogeneities may span a large range of length scales. These length scales can either differ by orders of magnitude (i.e. they are separated) or they may vary almost continuously in order of magnitude (i.e. they are continuous) [28]. It should be noted that the pore sizes are usually unevenly distributed in the sample and change over time, affecting heat flows, substances of reagents and products through a porous medium. Concentration and heat dispersion is caused by fluctuations in mass and heat flux, while diffusion is caused by molecular motion. A number of works have shown the importance of dispersion terms in averaged equations along with molecular diffusion. Various models of thermal dispersion have been developed in [29–35]. While the molecular diffusion takes place in a lowing and stagnant media as well, the dispersion is strongly influenced by the hydrodynamic flow. The dispersion was reported in the literature [28–34] with modelling as a tensor which components being either parallel or orthogonal to the main flow direction. The thermal and mass dispersion are affected by fluctuations of temperature and concentrations of species in multicomponent gas mixture in a porous media. It was shown [34] the significant effect of the thermal and mass dispersion on CCSO synthesis of micron barium titanate particles.

One of problems in sintering technology is to achieve the sufficiently low level of porosity. The Ti-$TiAl_3$ powder mixtures studied in [35, 36] allowed one to simultaneously achieve acceptable values of the sintered cathode porosity and cost of their manufacture under experimental industrial conditions. In [35–37] the models of sintering and synthesis of solid phase powder mixtures are considered, accounting for the mutual influence of the processes of volumetric changes in the sintering process. Temperature and concentration gradients lead to a change in the volume and appearance of displacements and stresses in the solid phase. The formula for variable porosity during CCSO was suggested in [23, 37]. The effect of volumetric changes in the synthesis of the barium-titanate including the thermal and mass dispersion was allowed predicting the characteristics of the combustion wave in the variable porosity of the sample. It should be noted that for the micron sizes of the synthesized particles, the characteristic values the Knudsen number is small and the effects of slippage and temperature jump [19] are negligible.

The models of synthesis of submicron particles using the CCSO [38–43] have specific features caused by comparatively high Knudsen number in gas that occupies the pores [19]. For submicron sizes of particles and pores, the effect of Knudsen layers in a gas near the surface of the pores is essential and the slip effects are required. Submicron models with slip conditions in combination with jumps of gas temperature and concentrations on the surface of pores were proposed, the macro-fluxes were obtained by averaging micro flows in pores.

3. Dimensionless governing equations

We consider the system of Janus like particles $(CoFe_2O_4/BaCO_3)(s)$ formation via carbon combustion using the following kinetics:

$$BaTiO_3(s) + CoFe_2O_4(s) + \alpha(C(s) + O_2(g)) + N_2(g) \rightarrow (CoFe_2O_4/BaTiO_3)(s) + \alpha CO_2(g) + N_2(g)\ 2 < \alpha < 14$$

We applied the reference time scale t_0, $t_0 = 10(s)$, related to activation energy E and pre-exponential factor in the reaction rate expression k_1 [34, 37]. The height and radius of the porous sample are $l_0 = 0.0007(m)$, $r_0 = 0.0.07(m)$, the gas velocity u_0 related to combustion speed in CCSO is $u_0 = 7 \cdot 10^{-4}\ (m/s)$ [25], $t_0 = k_1^{-1} \exp\left(E \times R^{-1} T_0^{-1}\right)$.

The dimensionless values marked by tilde for dimensional ones are presented below:

$$\tilde{x}_i = \frac{x_i}{l_0},\ \tilde{t} = \frac{t}{t_0},\ \tilde{u}_i = \frac{u_i}{u_0},\ \tilde{V}_{i,\text{solid}} = \frac{V_{i,\text{solid}}}{u_0},\ \tilde{p} = \frac{p}{p_0},\ u_0 = \frac{l_0}{t_0},\quad i = 1,2,3$$

$$\rho_{1g} = \rho_{O_2},\ \rho_{2g} = \rho_{CO_2},\ \rho_{3g} = \rho_{N_2},\qquad \rho_g = \rho_{1g} + \rho_{2g} + \rho_{3g}$$

$$\tilde{\rho}_g = \frac{\rho_g}{\rho_0},\ \tilde{\rho}_{jg} = \frac{\rho_{jg}}{\rho_0}, j = 1,2,3,\qquad \tilde{\rho}_{lS} = \frac{\rho_{lS}}{\rho_{0C}},\ \rho_S = \sum_{l=1}^{4}\rho_{lS},\quad l = 1,\ldots,4,\qquad \tilde{c}_{pg} = \frac{C_{pg}}{c_p},$$

$$\tilde{c}_{pg} = \frac{C_{pg}}{c_p},\ \tilde{D} = \frac{D}{D_0},\qquad \rho_{1g} = \rho_{O_2},\ \rho_{2g} = \rho_{CO_2},\ \rho_{3g} = \rho_{N_2},\qquad \rho_g = \rho_{1g} + \rho_{2g} + \rho_{3g},$$

$$\tilde{\rho}_g = \frac{\rho_g}{\rho_0},\ \tilde{\rho}_{jg} = \frac{\rho_{jg}}{\rho_0},\quad j = 1,2,3,\ \zeta_P = \frac{\rho_0}{\rho_{0C}},\ \tilde{\kappa}_0 = \frac{\kappa_0 t_0 A}{c_p \rho_0 V},\ \tilde{D}_m = \frac{D_m}{D_0},\ \tilde{\lambda}_g = \frac{\lambda_{\text{air}}}{\lambda_0},\ \tilde{\lambda}_S = \frac{\lambda_S}{\lambda_0},\ \tilde{c}_S = \frac{C_S}{c_p}$$

$$M_0 = m_{O2} + m_{CO2} + m_{N2},\qquad Ma^{-2} = \frac{\gamma_{air} p_0}{\rho_0 u_0^2},\ \text{Re} = \frac{l_0^2}{t_0 \nu_{air}},\qquad \text{R}_{\text{solid}} = p_0\left(\zeta_p \mu_{S0}\right)^{-1},$$

$$Pe_T = \frac{l_0^2 \rho_0 c_p}{t_0 \lambda_0},\ Pe_1 = \frac{l_0^2}{t_0 D_0},\ \tilde{Q} = \frac{Q t_0 k_1}{\rho_0 C_{pg} T_0},\ p_0 = \frac{R\rho_0 T_0}{M_0},\ \mu_0 = \rho_0 \nu_{\text{air}},\ \tilde{K} = \frac{K}{\mu_{S0}},\ \tilde{\mu}_{\text{solid}} = \frac{\mu_{\text{solid}}}{\mu_{S0}} \quad (1)$$

Here $A = \pi r_0^2$, $V = l_0 \times A$, $\rho_0 = \rho_{air} = 0.4$ (kg·m^{-3}), $\lambda_0 = \lambda_{air} = 0.06(W/m/K)$, $\rho_{0C} = 2267$ kg×m^{-3}, $D_0 = 2 \cdot 10^{-5}$ (m^2/s), $c_p = C_{p,air} = 1114(J/(kg \cdot K))$, $\nu_{air} = 9.7 \cdot 10^{-5}$ (m^2/s), $\rho_{1g} = \rho_{O2(g)}$, $\rho_{2g} = \rho_{CO2(g)}$, $\rho_{3g} = \rho_{N2(g)} \cdot \rho_{1s} = \rho_c$, $\rho_{2s} = \rho_{BaCO3}$, $\rho_{3s} = \rho_{CoFe2O4}$, $\rho_{4S} = \rho_{BaTiO3/CoFe2O4}$ are species densities, $\rho_g = \rho_{1g} + \rho_{2g} + \rho_{3g}$, $\rho_S = \rho_{1s} + \rho_{2S} + \rho_{3S} + \rho_{4S}$, $\rho = \chi\rho_g + (1\text{-}\chi)\rho_s$. $\tilde{\kappa}_0 = \kappa_0\, t_0 A / \left(c_p \rho_0 V\right)$ is the dimensionless heat transfer coefficient, $\tilde{c}_S, \tilde{c}_{pg}$ are the the heat capacities, $\tilde{\lambda}_S, \tilde{\lambda}_g$ are the heat conductivities, $\tilde{D}$ is the mass diffusivity, $p_0 = \frac{R\rho_0 T_0}{M_0}$ where p_0 and M_0 are the reference pressure and molar mass. *Ma*, Re are the Mach and Reynolds numbers in gas, R_s is the analog of Reynolds number for solid phase, Pe_T, Pe_1 are the thermal and diffusion Peclet numbers, subscript air is referred to the air parameters at normal condition, $\mu_{S0} = 2\times10^9$ Pa. The temperatures of gas and solid phases T_g, T_s can be found using formulas $T_g = T_0\left(1 + \beta\tilde{T}_g\right), T_S = T_0\left(1 + \beta\tilde{T}_S\right)$. The main dimensionless parameters related to activation energy and combustion heat are $\beta = RT_0/E$, $\gamma = c_p T_0 \beta/Q$ [20]. *R*, *E*, *Q* are the gas constant, activation energy and combustion heat. In our numerical simulation, the following values are applied $\beta \approx 0.1$, $\gamma \approx 0.2$. ($T_0 \approx 900$ K), $k_1 = 10$, $k_2 = 0.5$, $k_3 = 0.1$, $Q_1 = 60$, $Q_2 = 01$.

4. Expansion coefficients

We apply the Duhamel-Neumann relations [36] of linear thermoelasticity theory. $\sigma_{ij} = 2\mu_{S1}\varepsilon_{ij} + \delta_{ij}\left(\mu_{S2}\sum_k \varepsilon_{kk} - K\omega\right)$ along with the formulas for tensor invariants: $\sum_k \sigma_{kk} = \left(2\mu_{S1} + 3\mu_{S2}\right)\sum_k \varepsilon_{kk} - 3K\omega$, where σ_{ij} is the stress tensor and ε_{ij} is the tensor of deformation, K is the isothermal modulus of compression, μ_{s1}, μ_{s2} are the **Lamé** parameters.

We suppose that the gas pressure is equal to the normal stress at the pore surface, i.e. $\sum_k \sigma_{kk} = 3p$, then $\sum_k \varepsilon_{kk} = \left(K\omega + p\right)\mu_S^{-1}$, where $\mu_s = 2/3 \cdot \mu_{s1} + \mu_{s2}$. If no external force acts on the solid surface then $\sigma_{ii} = 0$ and consequently $\sum_k \varepsilon_{kk} = K\omega\mu_S^{-1}$.

The value $\omega = \omega_T + \omega_g + \omega_s$ is total coefficient of volumetric expansion where ω_T is the value of thermal expansion $\omega_T = 3\alpha_T\left(-\frac{T_g}{T_g^0} + 1\right)$ and the values ω_g, ω_s are found using molar volumes $\nu_{\text{lg}} = \frac{M_{\text{lg}}}{\rho_{\text{lg}}}, \nu_{jS} = \frac{M_{jS}}{\rho_{jS}}$ occupied by gas and solid components [35–37] via the following relations $\overline{\alpha}_{lg} = \frac{1}{3}\frac{\nu_{lg}}{\sum_{l=1}^{3}\nu_{lg} + \sum_{j=1}^{4}\nu_{jS}}, l = 1, 2, 3,$

$\bar{\alpha}_{iS} = \frac{1}{3}\frac{\nu_{iS}}{\sum_{l=1}^{2}\nu_{\mathrm{lg}} + \sum_{j=1}^{4}\nu_{jS}}, i = 1,...,4$, $\omega_g = 3\left[\sum_{j=1}^{3}\alpha_{jg}\left(-B_{jg} + B_{jg}^0\right)\right]$ and $\omega_S = 3\left[\sum_{j=1}^{4}\alpha_{jS}\left(-B_{jS} + B_{jS}^0\right)\right]$, where $B_{\mathrm{lg}} = \frac{Y_{\mathrm{lg}}}{Y_{\mathrm{g,tot}}}$, $B_{jS} = \frac{Y_{jS}}{Y_{S,tot}}$, $Y_{\mathrm{lg}} = \frac{\rho_{\mathrm{lg}}}{M_{\mathrm{lg}}}$, $Y_{\mathrm{g,tot}} = \sum_{l=1}^{3} Y_{\mathrm{lg}}$ and $Y_{jS} = \frac{\rho_{jS}}{M_{jS}}$, $Y_{S,tot} = \sum_{j=1}^{4} Y_{jS}$, superscript zero refers to the corresponding concentrations at initial time instant.

The variation of porosity $\chi(t,x,r)$ is modelled as the ratio of gas elementary volume to total elementary volume, occupied by gas and solid $V_{\Sigma}(t, x, r) = \mathrm{V}_g(t,x,r) + V_S(t,x.r)$ as $\chi(t,x,r) = V_n(t,x,r)/V_{\Sigma}(t,x,r)$. We apply the result [23, 37] to simulate the variable porosity in the form

$$\chi(t,x,r) = \frac{\chi(0,x,r)\left(1+\omega_g(t,x,r)\right)}{\chi(0,x,r)\left(1+\omega_g(t,x,r)\right)+\left(1-\chi(0,x,r)\right)\left(1+E(t,x,r)\right)} \tag{2}$$

$E(t,x,r) = \sum_k \varepsilon_{kk}(t,x,r)$. Using the initial condition $t = 0$: $\chi(t,x,r) = \chi(0,x,r)$ the relation has to be imposed $\omega_g(0,x,r) = E(0,x,r)$. We denote below $\chi(0,x,r) = \chi_0$.

5. Basic equations

Based on the law of the acting masses, we write a system of kinetic equations. Since the number of moles in the reactions is not conserved, for the components of substances we have the corresponding equations for the conservation of matter in the gas and solid phases. The basic equations are applied in the form the allow the regular limit $\chi \to 0$ and $\chi \to 1$. The dimensionless variables Eq. (1) are used, symbol tilde is omitted. Conservation of mass for total gas and solid phase can be presented as:

$$\frac{\partial \chi\rho_g}{\partial t} + \nabla\cdot\left(\chi\rho_g\,\mathbf{u}\right) = J_{S\to g}, \frac{\partial\left(1-\chi\right)\rho_S}{\partial t} = -J_{S\to g},\ J_{S\to g} = \chi\left(1-\chi\right)\rho_{1S}\rho_{1g}k\ \exp\left(\frac{T_g}{\beta T_g + 1}\right)$$

Mass conservation for gas phase are applied using the mass dispersion [34] in the form

$$\frac{\partial \chi\rho_g C_1}{\partial t} + \nabla\cdot\left(\chi\rho_g C_1\mathbf{u}\right) = \nabla\cdot\left(\frac{\chi}{Pe_1}\rho_g\mathbf{D_{mg}}\nabla C_1\right) - \frac{M_{1g}}{M_S}J_{S\to g}\ ,\quad C_2 = 1 - C_1 - C_3$$

$$\frac{\partial \chi\rho_g C_3}{\partial t} + \nabla\cdot\left(\chi\rho_g C_3\mathbf{u}\right) = \nabla\cdot\left(\frac{\chi}{Pe_1}\rho_g\mathbf{D_{mg}}\nabla C_3\right)$$

The components of mass dispersion are as follows

$$\mathbf{D_{mg}} = \begin{pmatrix} D_{1m} & 0 \\ 0 & D_{2m} \end{pmatrix},\quad \mathrm{Pe_{1m}} = \frac{|u|\cdot d_p}{D_m},\ \mathrm{Pe_{2m}} = \frac{|v|\cdot d_p}{D_m}\ ,$$

$$D_{1m} = D_m\left(\xi + \varphi_1\left(\mathrm{Pe_{1m}}\right)\right)\ ,\quad D_{2m} = D_m\left(\xi + \varphi_2\left(\mathrm{Pe_{2m}}\right)\right)\ ,$$

$$C_1 = \rho_{1g}\rho_g^{-1}, C_2 = \rho_{2g}\rho_g^{-1}, C_3 = \rho_{3g}\rho_g^{-1}\ ,$$

$$\varphi_1\left(\mathrm{Pe_{1m}}\right) = \left(b_0\mathrm{Pe_{1m}} + b_1\mathrm{Pe_{1m}}\ln\mathrm{Pe_{1m}}\right)\ ,$$

$$\varphi_2\left(\mathrm{Pe_{2m}}\right) = \left(b_0\mathrm{Pe_{2m}} + b_1\mathrm{Pe_{2m}}\ln\mathrm{Pe_{2m}}\right) \tag{3}$$

Where b_0, b_1 are constants and ξ is pore tortuosity coefficient [34]. Then, mass conservation for solid phase can be presented as:

$$\frac{\partial\left(1-\chi\right)\rho_{1S}}{\partial t} = -J_{1S}\ ,\quad \frac{\partial\left(1-\chi\right)\rho_{2S}}{\partial t} = -\frac{M_{2S}}{M_{4S}}J_{2S}\ ,$$

$$\frac{\partial\left(1-\chi\right)\rho_{3S}}{\partial t} = -\frac{M_{3S}}{M_{4S}}J_{2S}\ ,\quad \frac{\partial\left(1-\chi\right)\rho_{4S}}{\partial t} = J_{2S}\ ,$$

$$J_{1S} = \chi\left(1-\chi\right)\rho_{1g}\rho_{1S}k_1\exp\left(T_S/\left(1+\beta_1 T_S\right)\right)\ ,$$

$$J_{2S} = \left(1-\chi\right)^2\rho_{2S}\rho_{3S}k_2\exp\left(T_S/\left(1+\beta_2 T_S\right)\right)$$

Momentum conservation for gas is presented as:

$$\frac{\partial \chi\rho_g\,\mathbf{u}}{\partial t} + \nabla\cdot\left(\chi\rho_g\,\mathbf{uu}\right) + \mathrm{Ma}^{-2}\nabla p = \mathrm{Re}^{-1}\nabla\cdot\boldsymbol{\tau} + S_V + \vec{J}_{slip}^{\,macro}$$

The gas field stresses read $\boldsymbol{\tau} = \mu\left[\nabla\mathbf{u} + \left(\nabla\mathbf{u}\right)^T - \frac{2}{3}\left(\nabla\cdot\mathbf{u}\right)\mathbf{I}\right]$ and the term of distributed resistance in pores is given as $\left(\mathbf{S_V}\right)_i = -u_i\kappa_i$, $\kappa_i = \alpha_i|\mathbf{u}| + \varsigma_i, i = 1,2,3$. The macro slip flux due to gas slip at the pore surface is written as $\vec{J}_{slip}^{\,macro} = A_u\mathbf{u}\sqrt{p\rho_g}$ [20, 21].

The momentum equation for moving solid phase is applied in simplified form neglecting the thermal effect of the stresses [23].

$$\frac{\partial(1-\chi)\rho_S \mathrm{v}_{solid}}{\partial t}+\nabla\cdot((1-\chi)\rho_S\ \mathrm{v}_{solid}\mathrm{v}_{solid})=\mathrm{R}_S^{-1}\nabla\cdot\sigma\ ,\quad \sigma_{ij}=2\mu_{S1}\varepsilon_{ij}+\delta_{ij}\left(\mu_{S2}K\omega\mu_S^{-1}-K\omega\right)\ ,$$

$\mathbf{v}_{solid}$ is the velocity of solid phase.

The equation of heat balance in the gas phase considering the effect of thermal dispersion [34]

$$\rho_g C_{pg}\chi\left(\frac{dT_g}{dt}+\mathrm{u}\cdot\nabla T_g\right)+c_g T_g J_{S\to g}=\nabla\cdot\left(\chi\frac{D_{Tg}}{Pe_{Tg}}\nabla T_g\right)+Q_{jump}^{macro}-\kappa\left(T_g-T_S\right)+Q_r$$

$$Q_{Tg}=Q_1 J_{S\to g}\ ,\qquad Q_{jump}^{macro}=A_T\sqrt{\rho_g p}\left(-T_g+T_S\right)\ ,\qquad \mathrm{D_{Tg}}=\begin{pmatrix}\lambda_{1g} & 0\\ 0 & \lambda_{2g}\end{pmatrix},$$

$$\lambda_{1g}=\lambda_g\left(\xi+\varphi_1\left(\mathrm{Pe}_{1t}\right)\right),\ \lambda_{2g}=\lambda_g\left(\xi+\varphi_2\left(\mathrm{Pe}_{2t}\right)\right)\ .$$

Thermal balance equation for solid phase accounting for gas solid heat exchange and combustion heat reads

$$\rho_S c_S\left(1-\chi\right)\left(\frac{\partial T_S}{\partial t}+\mathrm{V}_{solid}\cdot\nabla T_S\right)-c_S T_S J_{S\to g}=\nabla\cdot\left(\left(1-\chi\right)\frac{\lambda_S}{\mathrm{Pe}_{Ts}}\nabla T_S\right)+\kappa\left(T_g-T_S\right)+Q_r\ ,\quad Q_{Ts}=Q_{Tg}\ .$$

Heat transfer coefficient is used in Leveka's form [25, 44] $\kappa=\kappa_0\left(1+\mathrm{Re}_{loc}^{0.3}+\mathrm{Re}_{Tloc}^{0.3}\right)$, where $\mathrm{Re}_{loc}=\mathrm{Re}|\mathbf{u}|\rho_g$, is local Reynolds number and $\mathrm{Pe}_{Tloc}=\mathrm{Pe}_{Tg}, \mathrm{Pe}_T|\mathbf{u}|\rho_g$, are local Peclet numbers.

6. Results and discussion

The schematic combustion model ($0<r<1$, $0<z<\mathrm{L}$) is presented in Fig. 1A. The front moves from bottom to top. Oxygen is supplied from the bottom. Porous part of the reactor occupies the region $0<r<1-d$, $0<x<L$. Flow part of the reactor is $1-d<r<1$, $0<x<L$. The model accounts Janus like particles by determination of density of the solid phase during the densification.

The expansion coefficient is given as follows: K = 0.564

$$t=0:\bar{\alpha}_{lS}=\alpha_{lS}^0\ ,\quad \alpha_{1S}^0=0.018\ ,$$

$$\alpha_{2S}^0=0.653/\mathrm{K}_\alpha\ ,\quad \alpha_{3S}^0=2.915/\mathrm{K}_\alpha\ ,$$

$$\alpha_{4S}^0=0.295/\mathrm{K}_\alpha\ ,\quad \alpha_T=\alpha_T^0=5\cdot10^{-5}\qquad (4)$$

The simulation of variable porosity is presented for $\mathrm{K}_\alpha = 1$ and $\mathrm{K}_\alpha = 6$. We report the ($CoFe_2O_4$/$BaCO_3$)(s) synthesis using carbon combustion temperature jump at pore surface [24, 25] and chemical heating is applied in the form:

simulation in a sample with submicron pores. The results of computation of combustion presented below refer to the values of parameters as follows. For simplicity $\sum_{k=1}^{3}\varepsilon_{kk}=\omega$, $\gamma \approx 0.28$, $\chi = 0.05$–0.5, $\beta_1 = 0.086$ and $\beta_2 = 0.136$. The dimensionless resistance of porosity is given as $\alpha_i = 0$ and $\varsigma_i = 50$. The Mach and Reynolds number are $Ma_0 = 0.2$ and $\mathrm{Re}_0 = 10^{-2}$. The values of temperature correspond to our experimental data for porosity of 12%. The ignition temperature $\mathrm{T}_{init} = 0$, ($\mathrm{T}_{init,\mathrm{dim}} = 580$ C) and the wall temperature $\mathrm{T}_W = -0.19$, ($\mathrm{T}_{w,dim} = 570$ C) are prescribed. The value of initial dimensionless temperature $\mathrm{T}_{inital} = -10.6$, $t = 0$ corresponds to the room temperature. The temperature jump and gas velocity slip were imposed using $A_T = 10$ and $A_u = 100$ [24], for which the simulation of carbon combustion in submicron pores is in a satisfactory agreement with experiment.

The results of CCSO modelling for the micron sized reagents and products were obtained for the following parameters [24, 25]: $\alpha_j = 0$, $\varsigma_i = 50$, $t_{init} = 0.25$, $Ma = 0.01$, $Q_f = 500$, $Q = 60$, $Re = 0.1$, $Pe_{Tg} = 0.2$, $Pe_{Ts} = 0.4$, $\mathrm{Pe}_1 = 0.72$. The cylindrical sample was placed in vertical position. The ignition initiated at the bottom z = 0. In the figures below $0\le r\le 1$, $0\le z\le L$ using cylin-

drical coordinates r, z; where $r = 0$ is the axis of symmetry.

The density of Janus particle ($CoFe_2O_4/BaCO_3$) (s) resulted in sintering in the reactor ($0<r<1$, $0<z<L$) is presented at various time instances for small porosity in Fig. 1 and large one in Fig. 2. The carbon ignition is initiated from the bottom. In figures below the r- axis is horizontal and the z- axis is vertical one. At initial instant the amounts of 45 wt.% of $BaTiO_3$, 45 wt.% of $CoFeO_4$ and 10 wt.% of carbon in the mixture are given. At the final stage, all carbon is transformed to CO_2 and the amount of product of sintering ($CoFe_2O_4/BaCO_3$) (s) in the mixture will be 90% and 10% of CO_2. This value of 90% corresponds to totally synthesized product. The duration of total synthesis strongly depends on the porosity of the sample.

The data demonstrate the result of simulation of submicron JP synthesis taking into account the slippage $\vec{J}_{slip}^{macro} = A_u \mathbf{u}\sqrt{p\rho_g}$, $A_u = \dfrac{\theta}{2-\theta}\sqrt{\dfrac{2}{\pi}}$ and temperature jump $Q_{jump}^{macro} = A_T\sqrt{\rho_g p}\left(-T_g + T_S\right)$, $A_T = \dfrac{\alpha'}{2-\alpha'}\sqrt{\dfrac{2}{\pi}}\dfrac{c_P + c_V}{2c_P}$ of gas at solid surface where θ, ($0\le\theta\le1$) is the reflection coefficient and α', ($0\le\alpha'\le1$) is the thermal accommodation coefficient. The simulation at constant porosity is presented neglecting the mass and temperature dispersion that is not significantly influence on heat and mass interphase exchange.

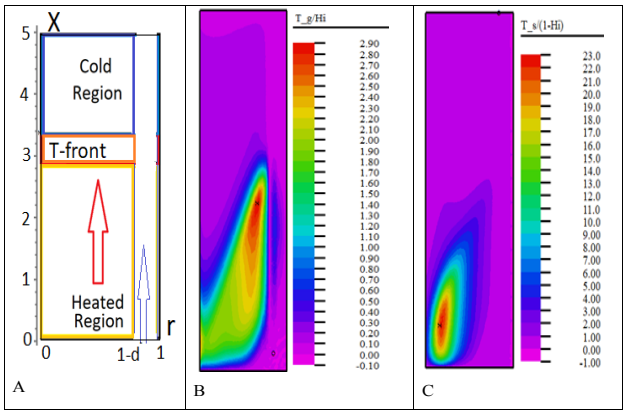

Fig. 1. (A) – The schematic representation of the combustion model. The front moves from bottom to top. Oxygen is supplied from the bottom. Porous part of the reactor occupies the region $0<r<1-d$, $0<x<L$. Flow part of the reactor is $1-d<r<1$, $0<x<L$. (B) – The dimensionless temperature of gas phase $\tilde{T}_g(t,x_j,r)$ and (C) – solid $\tilde{T}_S(t,x_j,r)$ at time instance $t = 0.3$ is shown for initial porosity χ_0 and expansion.

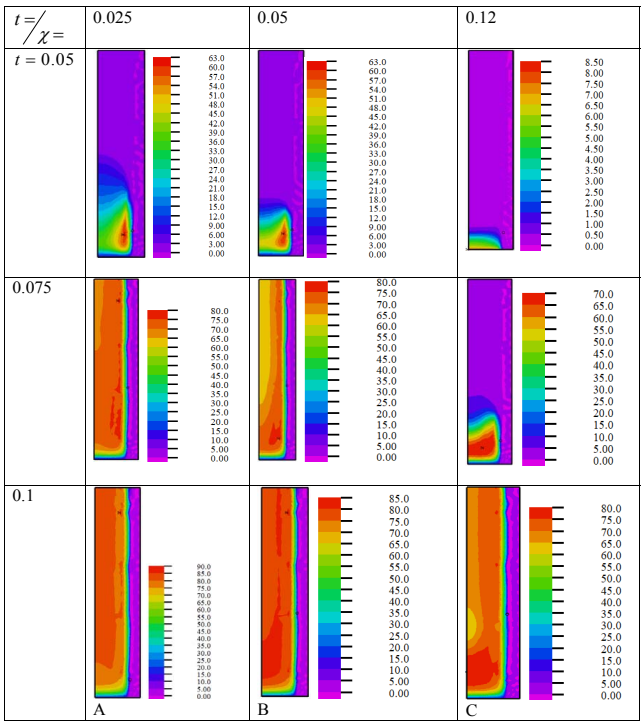

Fig. 2. The amount of sintered $CoFe_2O_4/BaTiO_3$ for small porosity χ = 0.025, 0.05, 012 at time instances t = 0.05, 0.075, 0.1, it is shown for the reactor region $0<r<1$, $0<z<L$.

Figure 2 shows that the increasing of synthesis rate when the porosity is decreasing (compare to the $CoFe_2O_4/BaTiO_3$ amount in columns A, B, and C). The highest synthesis rate is found for porosity χ = 0.025 (A) as compared to χ = 0.05, 0.12 (B, C), respectively. Note that 90%, 85% and 80% of product is synthesized at time instance of t = 0.1 for porosity χ = 0.025, 0.05 and χ = 0.12, respectively. The uniformity of product increases in time that is shown at t = 0.075 and t = 0.1 in column B. More rapid synthesis takes place in more heated zone. Initially the region of rapid sintering is located rather far from the axis of symmetry r = 0, because the ignition initiated by oxygen flux along the lateral surface of a sample [18]. This region is demonstrated in columns A and B at t = 0.05.

The results for larger porosity is presented in Fig. 3. The almost uniform 90% distribution of $CoFe_2O_4/BaTiO_3$ is found for $\chi = 0.2$ at $t = 0.2$. Note that sintering is rather slow for $\chi = 0.5$ and located at t = 0.2 in the heated zone (B) of combustion for χ = 0.5. Figure 3 demonstrates the thermal wave propagating upwards. The variation in time of gas temperature at time instances t = 0.05, 0.1, 0.15 are presented. Note the temperature maximum is located in the region close to symmetry axis. At t = 0.15 the fabrication of 90% of uniform $CoFe_2O_4/BaTiO_3$

product was obtained at negligibly low amount of carbon in the mixture and 10% of CO_2. The maximal temperature of 1375 K is attained. Note that experimental measurement at the instance of totally consumed carbon results in temperature of T = 1381 K in a region close to the reactor center. Figure 4 shows the diminishing of the carbon combustion front speed with increasing the porosity of the sample.

The data in Figs. 5–10 showed the result of simulation of micron JP synthesis for which the slippage and temperature jump of gas at solid surface can be neglected. The simulation for variable porosity is presented using the Eq. (2) and taking into account the mass $D_{1m} = D_m\,(\xi + \varphi_1\,(\mathrm{Pe}_{1\mathrm{m}}))$, $D_{2m} = D_m\,(\xi + \varphi_2\,(\mathrm{Pe}_{2\mathrm{m}}))$, $\varphi_1\,(\mathrm{Pe}_{1\mathrm{m}}) = (b_0\mathrm{Pe}_{1\mathrm{m}} + b_1\mathrm{Pe}_{1\mathrm{m}}\ln\mathrm{Pe}_{1\mathrm{m}})$, $\varphi_2\,(\mathrm{Pe}_{2\mathrm{m}}) = (b_0\mathrm{Pe}_{2\mathrm{m}} + b_1\mathrm{Pe}_{2\mathrm{m}}\ln\mathrm{Pe}_{2\mathrm{m}})$, and temperature dispersion $\lambda_{1\mathrm{g}} = \lambda_{\mathrm{g}}\,(\xi + \varphi_1\,(\mathrm{Pe}_{1t}))$, $\lambda_{2g} = \lambda_g\,(\xi + \varphi_2\,(\mathrm{Pe}_{2t}))$ that significantly influence on heat and mass interphase exchange [34]. The thermal and mass dispersion in JP synthesis was simulated for $b_1 = 0$ according to the Eq. (3), and particle diameter $d_p = 3 \cdot 10^{-4}(m)$. The pairs of curves (1, 4), (2, 5), (3, 6) in Fig. 6C show the volume solid phase time history at the positions with coordinates (0, 0.5), (0.15, 0.5), (0.75, 0.5) respectively. The pairs of curves (1, 4), (2, 5), (3, 6) in Fig. 7C show the porosity time history at the positions with coordinates (0, 0.5), (0.15, 0.5), (0.75, 0.5) respectively.

Figure 9 demonstrates the effect of expansion on velocity of solid. The large expansion coefficients cause the radial and axial solid velocities that presented in Fig. 9B, D that are about an order of magnitude higher compared to small expansion solid velocities (Fig. 9A, C). These solid velocities effect on the advection heat transfer in solid phase as well as on gas temperature distribution due to interphase heat exchange. The concentration expansion of the gas phase due to the gas pressure at the surface of the pores slows the reduction of the pore's sizes during the combustion process due to the thermal and concentration expansion of solid

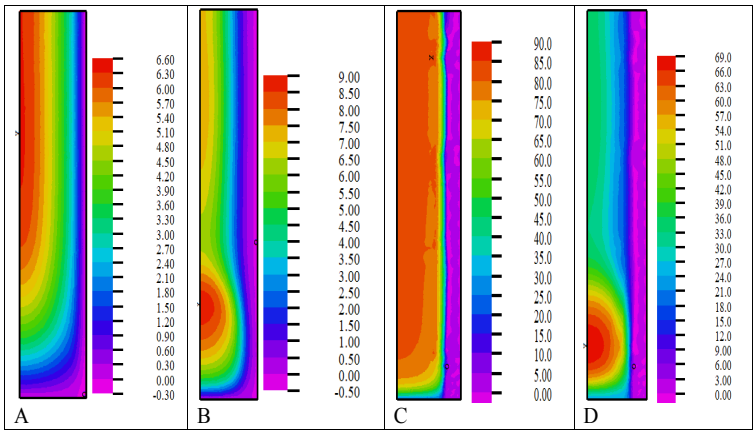

Fig. 3. Gas temperature for (A) – $\chi = 0.2$; (B) – $\chi = 0.5$; and amount of $CoFe_2O_4/BaTiO_3$ for C – $\chi = 0.2$ and (D) – $\chi = 0.5$ at $t = 0.2$ are shown.

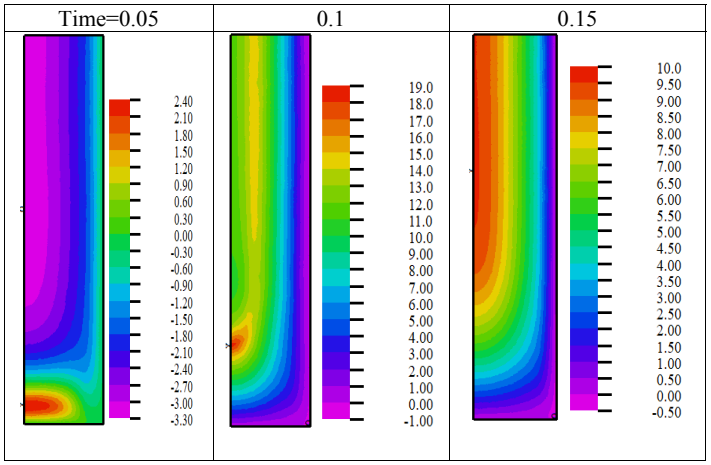

Fig. 4. Gas temperature for $\chi = 0.12$ at time instances at 0.05, 0.1, 0.15 is presented.

phase. The results obtained show a significant effect of volumetric changes in the solid phase. The proposed model allows us to analyze the effect of thermal and concentration expansion on the rate of synthesis and the distribution of the product in the synthesized area.

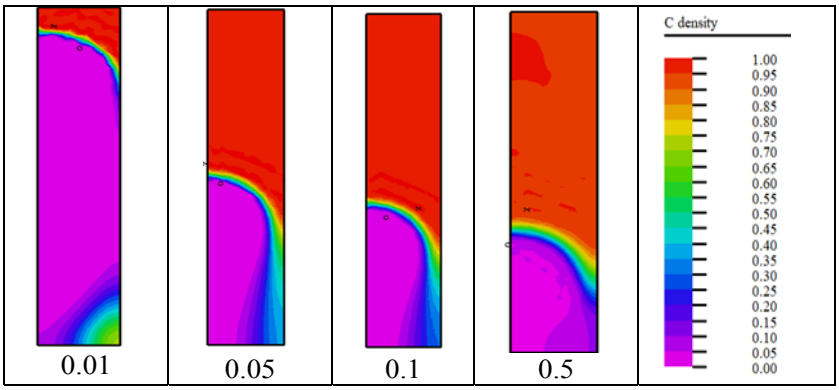

Fig. 5. The dependence of combustion front propagation rate on porosity. Carbon density for χ = 0.01, 0.05, 0.1, 0.5, respectively at time instance t = 0.5.

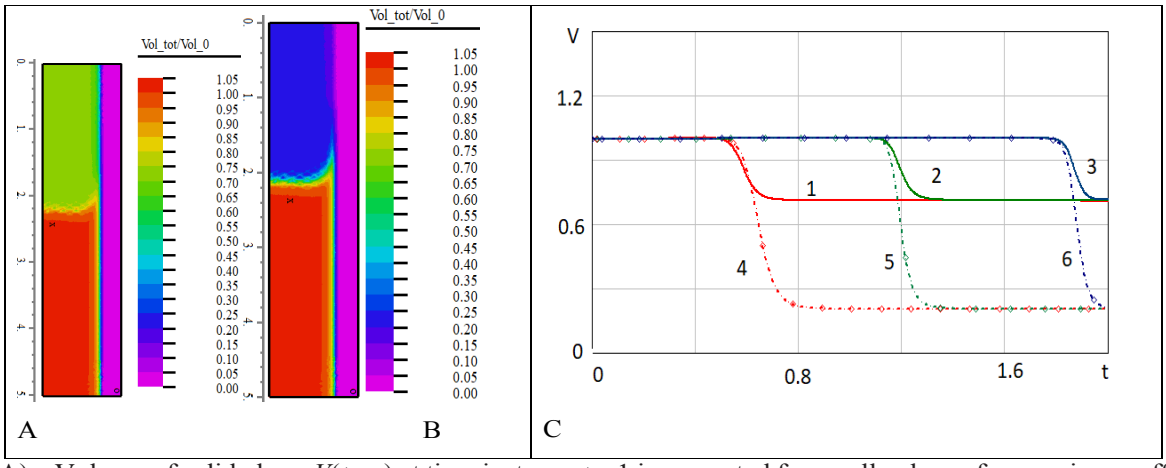

Fig. 6. (A) – Volume of solid phase $V(t,x,r)$ at time instance t = 1 is presented for small values of expansion coefficients and (B) – for large expansion coefficients; (C) – demonstrates the volume of solid phase $V(t, x, 0.25)$ versus time at the positions (x_j, 0.25). Solid curves and symbols are referred to large expansion coefficients for K_α = 1 and small expansion coefficients at K_α = 6 according to the Eq. (4).

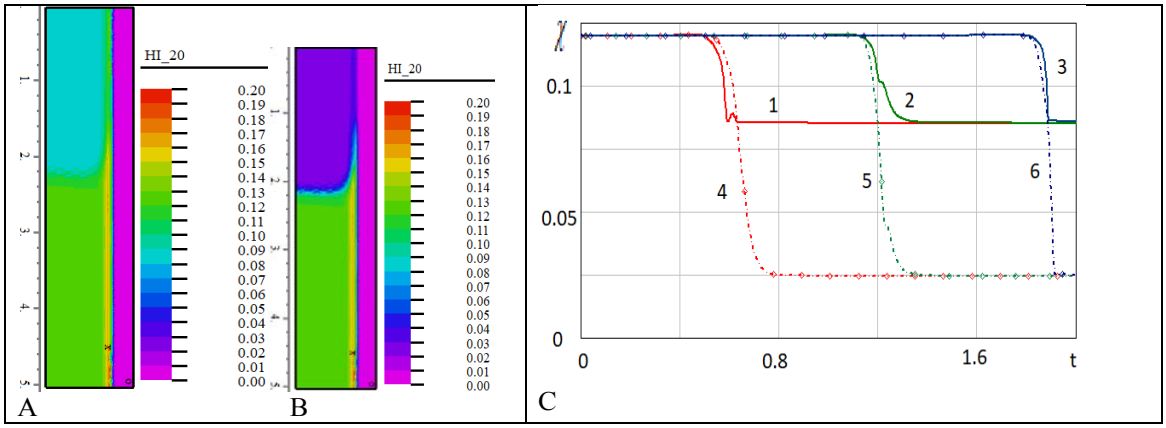

Fig. 7. (A) – Porosity $\chi(t,x,r)$ at time instance t = 1 is presented for small values of expansion coefficients and (B) – large expansion coefficients; (C) – demonstrates the porosity $\chi(t,x_j, 0.25)$ versus time at the positions (x_j, 0.25). Solid curves and symbols are referred to large expansion coefficients at K_α = 1 and small expansion coefficients at K_α = 6 according to the Eq. (4).

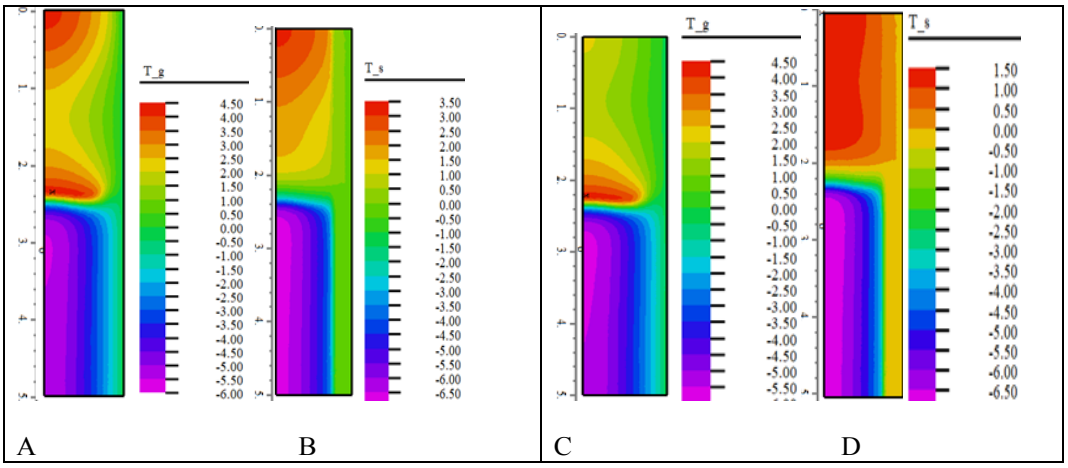

Fig. 8. (A and C) – Temperature of gas and (B and D) – temperature of solid is shown for small expansion coefficients (A, B) and large expansion coefficients (C, D).

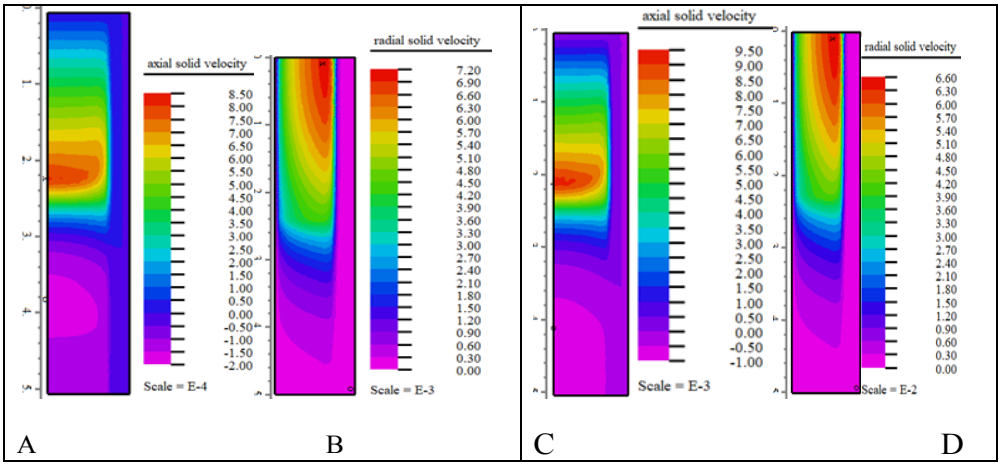

Fig. 9. (A, C) – Axial velocity of solid and (B, D) – radial velocity of solid is shown for small expansion coefficients (A, B) and large expansion coefficients (C, D).

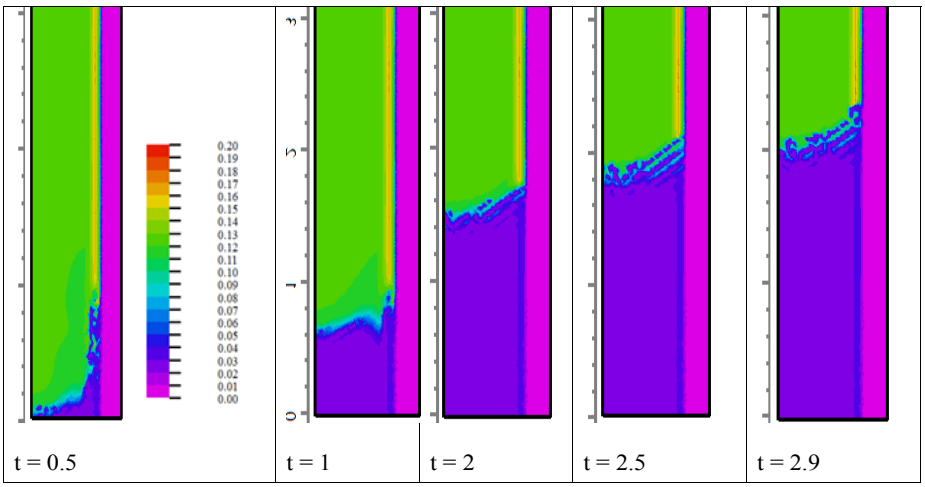

Fig. 10. The porosity distribution in the reactor at time instances t = 0.5, 1, 2, 2.5, 2.9, respectively.

The results presented in this paper allow us to reveal the features of the influence of Knudsen layers on the heat and mass transfer in JP densification and qualitatively agree with results [20, 21]. The magnitudes of the jumps in the temperature and concentrations of the components of the gas phase are determined by the coefficient of heat – accommodation of molecules and thermal diffusion. The amount of slip depends on the coefficient of the reflection of molecules from the walls of the reactor

of JP synthesis and form surface of pores. An intense gas flow from the combustion zone and from the sample causes heat loss and slows down the combustion process during the densification. In the present paper, we consider only the densification of Janus-like particles in the porous media.

7. Conclusions

The combustion model allows to predict the formation rate of JP densification using CCSO and analyse the homogeneity of the product for various initial porosity of reagent mixture. The uniformity of product increases during the combustion time. More rapid synthesis of JP takes place in the combustion zone. Initially the region of rapid densification is located rather far from the axis of symmetry $r = 0$, because the ignition initiated by oxygen flux along the lateral surface of a sample. The model predicts that 90%, 85% and 80% of product is synthesized at the instance time $t = 0.1$ for porosity of $\chi = 0.025$, 0.05, and 0.12, respectively. The larger porosity the lower the rate of JP formation during the combustion sintering. The temperature field caused by the thermal wave propagation in the sample significantly varies in space and time and considerably affects the synthesis process as it is demonstrated. The variable porosity strongly depends on volumetric expansion of the sample. The model of volumetric expansion in densification JP allows us to achieve the JP of sufficiently low porosity compared to one at initial time instance. The generalization of the two-temperature model using variable porosity formula is presented for self-consistent calculation of the coefficients for concentration expansion, thermal and mass dispersion. The expansion coefficients are calculated in the porous zone of the reactor in accordance with the kinetics of JP synthesis, the given initial values of the density and expansion coefficients of the reactants in the gas and solid phases.

Acknowledgements

AAM acknowledges supported in the framework of governmental program for IPMech RAS topic no AAAA-A20-120011690135-5 and KSM acknowledges the NSF PREM award No. DMR-1523577 and DMR-2122178.

References

[1]. C. Casagrande, P. Fabre, E. Raphaël, M. Veyssie, *Europhys Lett.* 9 (1989) 251–255. DOI: 10.1209/0295-5075/9/3/011

[2]. S. Pradhan, L. Xu, S. Chen, *Adv. Funct. Mater.* 17 (2007) 2385–2392. DOI: 10.1002/adfm.200601034

[3]. S. Granick, S. Jiang, Q. Chen, *Phys. Today* 62 (2009) 68–69. DOI: 10.1063/1.3177238

[4]. A. Walther, A. Müller, *Chem. Rev.* 113 (2013) 5194–5261. DOI: 10.1021/cr300089t

[5]. N. Zhao, M. Gao, *Adv. Mater.* 21 (2009) 184–187. DOI: 10.1002/adma.200800570

[6]. J. Zhang, B.A. Grzybowski, S. Granick, *Langmuir* 33 (2017) 6964–6977. DOI: 10.1021/acs.langmuir.7b01123

[7]. T.C. Le, J. Zhai, W.-H. Chiu, P.A. Tran, N. Tran, *Int. J. Nanomed*. 14 (2019) 6749–6777. DOI: 10.2147/IJN.S169030

[8]. C. Trevino De Leo, G.C. Dannangoda, M.A. Hobosyan, J.T. Held, F. Safi Samghabadi, M. Khodadadi, D. Litvinov, K.A. Mkhoyan, K.S. Martirosyan, *Ceram. Int*. 47 (2021) 5415–5422. DOI: 10.1016/j.ceramint.2020.10.123

[9]. M. Nair, R. Guduru, P. Liang, J. Hong, V. Sagar, S. Khizroev, *Nat. Commun.* 4 (2013) 2729. DOI: 10.1038/ncomms3729

[10]. A. Perro, S. Reculusa, S. Ravaine, E. Bourgeat-Lami, E. Duguet, *J. Mater. Chem*. 15 (2005) 3745–3760. DOI: 10.1039/b505099e

[11]. S. Betal, A.K. Saha, E. Ortega, M. Dutta, A.K. Ramasubramanian, A.S. Bhalla, R. Guo, *Sci. Rep.* 8 (2018) 1755. DOI: 10.1038/s41598-018-20191-w

[12]. F.S. Samghabadi, L. Chang, M. Khodadadi, K.S. Martirosyan, D. Litvinov, *APL Mater*. 9 (2021) 021104. DOI: 10.1063/5.0036518

[13]. G.E. Karniadakis, A. Beskok, N.R. Aluru (2005). Microflows and Nanoflows Fundamentals and Simulation. In Interdisciplinary Applied Mathematics (pp. 1–61). (Interdisciplinary Applied Mathematics; Vol. 29). Springer.

[14]. J.K. Holt, H.G. Park, Y. Wang, M. Stadermann, A.B. Artyukhin, C.P. Grigoropoulos, A. Noy, O. Bakajin, *Science* 312 (2006) 1034–1037. DOI: 10.1126/science.1126298

[15]. J. Eijkel, *Lab. Chip.* 7 (2007) 299–301. DOI: 10.1039/B700364C

[16]. A.I. Erofeev, M.N. Kogan, O.G. Fridlender, *Fluid Dynam*. 45 (2010) 134–146. DOI: 10.1134/S0015462810010151

[17]. M. Kurzyp, C.A. Mills, R. Rhodes, T.R. Pozegic, C.T.G. Smith, M.J. Beliatis, L.J. Rozanski, A. Werbowy, S.R.P. Silva, *J. Phys. D: Appl. Phys.* 48 (2015) 115305. DOI: 10.1088/0022-3727/48/11/115305

[18]. V.Ya. Rudyak, A.A. Belkin, V.V. Egorov, D.A. Ivanov, *Nanosystems: Phys. Chem. Math.* [Nanosistemy: fizika, himiâ, matematika] 2 (2011) 100–112 (in Russian).

[19]. A.A. Markov, *Comput. Fluids* 99 (2014) 83–92. DOI: 10.1016/j.compfluid.2014.04.012

[20]. A.A. Markov, I.A. Filimonov, K.S. Martirosyan, *J. Comput. Phys.* 231 (2012) 6714–6724. DOI: 10.1016/j.jcp.2012.06.003
[21]. A.A. Markov, M.A. Hobosyan, K.S. Martirosyan, *Physical-Chemical Kinetics in Gas Dynamics* 16 (2015). http://chemphys.edu.ru/issues/2015-16-1/articles/506/
[22]. Y. Daghighi, Y. Gao, D. Li, *Electrochim. Acta* 56 (2011) 4254–4262. DOI: 10.1016/j.electacta.2011.01.083
[23]. A.A. Markov. *PNRPU Bulletin. Chemical Technology and Biotechnology* 2 (2020) 160–177 (in Russian). DOI: 10.15593/2224-9400/2020.2.12
[24]. A.A. Markov, M.A. Hobosyan, K.S. Martirosyan, *Nanoscience and Technology: An International Journal* 6 (2015) 209–222. DOI: 10.1615/NanomechanicsSciTechnolIntJ.v6.i3.40
[25]. A.A. Markov, I.A. Filimonov, K.S. Martirosyan, *Theor. Found. Chem. Eng.* 51 (2017) 27–37. DOI: 10.1134/S0040579517010134
[26]. B.A. Boley, J.H. Weiner, Theory of Thermal Stresses, Dover Publications, 2011, ISBN 10: 0486695794
[27]. E.A. Olevsky, *Mater. Sci. Eng. R Rep* 23 (1998) 41–100. DOI: 10.1016/S0927-796X(98)00009-6
[28]. S. Whitaker, *Chem. Eng. Sci.* 28 (1973) 139–147. DOI: 10.1016/0009-2509(73)85094-8
[29]. C.T. Hsu, P. Cheng, Int. *J. Heat Mass Transf.* 33 (1990) 1587–1597. DOI: 10.1016/0017-9310(90)90015-M
[30]. M. Fatehi, M. Kaviany, *Int. Heat Mass Transfer.* 11 (1997) 2607–2620. DOI: 10.1016/S0017-9310(96)00282-7
[31]. A.A.M. Oliveira, M. Kaviany, *Prog. Energ. Combust. Sci.* 27 (2001) 523–545. DOI: 10.1016/S0360-1285(00)00030-7
[32]. F.M. Pereira, A.A.M. Oliveira, F.F. Fachini, *J. Fluid Mech.* 657 (2010) 285–307. DOI: 10.1017/S0022112010001461
[33]. J.M.P.Q. Delgado, *Chem. Eng. Res. Des.* 85 (2007) 1245–1252. DOI: 10.1205/cherd07017
[34]. A.A. Markov, *Physical-Chemical Kinetics in Gas Dynamics* 20 (2019) 1–14. DOI: 10.33257/PhChGD.20.4.870
[35]. S.N. Sorokova, A.G. Knyazeva, *Physical mezomechanics* 11 (2008) 95–101 (in Russian).
[36]. S.N. Sorokova, A.G. Knyazeva. Related model of sintering the powders of the TI-TIAI3 system. Bulletin of the Tomsk Polytechnic University 314 (2009) 96–101 (in Russian).
[37]. A.A. Markov, *Physical-Chemical Kinetics in Gas Dynamics* 22 (2021) 1–21 (in Russian). DOI: 10.33257/PhChGD.22.1.924
[38]. K.S. Martirosyan, E. Galstyan, S. M. Hossain, Yi-Ju Wang, D. Litvinov, *Mater. Scie. Eng. B* 176 (2011) 8–13. DOI: 10.1016/j.mseb.2010.08.005
[39]. K.S. Martirosyan, D. Luss, *Ind. Eng. Chem. Res.* 46 (2007) 1492–1499. DOI: 10.1021/ie0605711
[40]. K.S. Martirosyan, M. Iliev, D. Luss, *Int. J. Self-Propag. High-Temp. Synth.* 16 (2007) 36–45. DOI: 10.3103/S1061386207010050
[41]. K.S. Martirosyan, L. Chang, J. Rantschler, S. Khizroev, D. Luss, D. Litvinov, *IEEE T. Magn.* 43 (2007) 3118–3120. DOI: 10.1109/TMAG.2007.893844
[42]. K.S. Martirosyan, D. Luss, *AIChE J.* 51 (2005) 2801–2810. DOI: 10.1002/aic.10528
[43]. K.S. Martirosyan, C. Dannangoda, E. Galstyan, D. Litvinov, *J. Appl. Phys.* 111 (2012) 094311. DOI: 10.1063/1.4711097
[44]. D.A. Frank-Kamenetskii, Diffusion and Heat Transfer in Chemical Kinetics (Second Enlarged and Revised Edition), Translation Editor: J.P. Appleton, Plenum Press, 1969.

List of principal notations

T_0 = 1000 °C	Referred temperature
T'	Dimensional temperature
$T = \frac{T'}{T_0}$	Dimensionless temperature
$\tilde{T} = \frac{T-1}{\beta}$	Dimensionless normalized temperature
T_g, T_{jS}	Gas temperature and solid phase temperature
T_{init} = 450–500 C	Ignition temperature
$T_{initial}$ $T_{initial} = -1/\gamma$	Initial temperature of the sample
c_{pk}	Specific capacity at constant pressure
ρ_{lg}, l = 1,2, 3	Densities of gas species
$\rho_g = \rho_{1g} + \rho_{2g} + \rho_{3g}$	Density of gas mixture
$\nu_{jS} = \frac{M_{jS}}{\rho_{jS}}$	Molar volume of solid component
$\omega = \sum_{k=1}^{3} \varepsilon_{kk}$	First invariant of deformation tensor Pa
σ_{ij}	Stress tensor for solid phase Pa
$\sum_k \sigma_{kk} = (2\mu_{S1} + 3\mu_{S2}) \sum_k \varepsilon_{kk} - 3K\omega$	Thermo-elasticity relation Pa
$\sigma_{ij} = 2\mu_{S1}\varepsilon_{ij} + \delta_{ij}\left(\mu_{S2}\sum_k \varepsilon_{kk} - K\omega\right)$	Duamel-Neuman formulas
$\omega = \omega_T + \omega_g + \omega_S$	Total expansion (dimensionless)
μ_{S1}, μ_{S2}	Lame coefficients *Па*
ω_g, ω_S	Concentration expansions
ω_T	Thermal expansion
E_1, E_2 K	Activation energy Volumetric expansion coefficient Pa
$\overline{\alpha}_{ig}$, $\overline{\alpha}_{iS}$	Species expansion coefficients
$\beta_k = \frac{RT_0}{E_k}, k = 1,2$ $\gamma = \frac{c_P T_0 \beta_1}{Q_1}$	Dimensionless parameters
ε_{ij}	Tensor of deformations (dimensionless)

$Pe_l = \frac{u_0 l_0}{D_{l,0}}, l = 1,2$, $Pe_T = \frac{u_0 l_0}{\lambda_0}$	Peclet numbers
$u_0 = \frac{l_0}{t_0}$	Referred velocity
$\mathrm{Re}_0 = \frac{u_0 l_0 \rho_0}{\mu_0}$	Reynolds number
R_{Solid}	The Reynolds number analog for solid phase
χ	Porosity coefficient
κ	Thermal transfer coefficient
P_0	Referred pressure
μ_0	Referred gas viscosity
λ_0	Referred thermal conductivity
Ma_0	Mach number
M_{1g}, M_{2g}, M_{jS}, j = 1,...,4	Molar masses
Q_f	Thermal flux
Q_1, Q_2 $Q_{Tg}, Q_{Ts}, Q_{jump}^{macro}$	Combustion heat Heat fluxes due to chemical reaction and temperature jump
$A_u = \frac{\theta}{2-\theta}\sqrt{\frac{2}{\pi}}$ $\vec{J}_{slip}^{macro} = A_u \mathbf{u}\sqrt{p\rho_g}$	Slip parameters
θ, $(0 \le \theta \le 1)$	Reflection coefficient
A_T; $Q_{jump}^{macro} = A_T\sqrt{\rho_g p}\left(-T_g + T_S\right)$ $A_T = \frac{\alpha'}{2-\alpha'}\sqrt{\frac{2}{\pi}}\frac{c_P + c_V}{2c_P}$	Temperature jump parameter
α', $(0 \le \alpha' \le 1)$	Thermal accommodation coefficient
D_T	Thermal diffusivity coefficient
R = 8.314	Gas constant
$t_0 = \frac{\exp\left(E/RT_0\right)}{k}$, $l_0 = \sqrt{\lambda_0 t_0 / (c_V \rho_0)}$	Referred time and length scales for the Frank-Kamenetskii variables
t_{init}	Ignition time
Subscripts: g, s	Gas and solid